

*Supplement of*  
**Retrieval of the Sea Spray Aerosol Mode from Submicron Particle  
Size Distributions and Supermicron Scattering during LASIC**

Dedrick et al.

5

*Correspondence to:* Lynn M. Russell (lmrussell@ucsd.edu)

**Contents of this file**

1. Text S1 to S2
2. Figures S1 to S6
- 10 3. Table S1

## Text S1. Selecting the Most Probable Mie Solutions

Since many solutions are within the constraints of three wavelengths of measurements, we applied a low error restriction on Mie solutions to consider only the most probable fitting parameters ( $N_T$ ,  $D_g$ ,  $\sigma_g$ ) based on their frequency of occurrence. The normalized probabilities of the fitting parameters from Mie solutions that fall below the scattering error threshold,  $\Delta\sigma_{sca,RGB}$ , for one retrieval during LASIC are shown in Fig. S3a-c. This retrieval was selected as its  $\Delta\sigma_{sca,RGB}$  was within the average value for all LASIC observations ( $3.1 \pm 2.1 \text{ Mm}^{-1}$ ) and is representative of most cases assessed.

Mie solutions that meet the error threshold constrained the mode number ( $N_T$ ) and mean diameter ( $D_g$ ) of the sea spray mode as shown by likely (probability > 75%)  $N_T$  and  $D_g$  falling within narrow ranges of the low error solutions (4% and 10% of the sample space respectively) compared to a less constrained range for  $\sigma_g$  (45% of the sample space). Since  $\sigma_g$  had a wider range of probable values, this parameter was effectively constrained by considering the joint probabilities of  $N_T|\sigma_g$  and  $D_g|\sigma_g$ . These probabilities were computed as

$$P(N_T, \sigma_g) = P(N_T|\sigma_g) \cdot P(\sigma_g) \quad (1)$$

25

$$P(D_g, \sigma_g) = P(D_g|\sigma_g) \cdot P(\sigma_g) \quad (2).$$

The highest joint probability values restricted solutions to localized regions of the solution space (Fig. S3d-e). Selecting only the upper 5<sup>th</sup> normalized probability percentile of joint probabilities further restricted the full Mie solution sample space by an additional 16% and 13% for  $N_T|\sigma_g$  and  $D_g|\sigma_g$ , respectively (red dots in the contour plots). We next examined the retrieved sea spray modal properties by applying the joint probability restrictions to all observations during the clean marine background season of LASIC and compared the results (Fig. S4). Restricting low error solutions using  $D_g|\sigma_g$  joint probability led to retrieved sea spray masses that were 40 – 60% higher than the  $N_T|\sigma_g$  combination, had mean mass diameters smaller than  $N_T|\sigma_g$  ( $0.59 \pm 0.08 \mu\text{m}$  vs.  $1.02 \pm 0.15 \mu\text{m}$ ), and much broader mode widths ( $3.42 \pm 0.25$  vs.  $2.06 \pm 0.24$ ). Although the retrieved mass mean diameters using the  $D_g|\sigma_g$  joint probability were within the range of reported values from literature (Table 4), the exceptionally broad widths outside of the reported range suggests that the restriction using  $D_g|\sigma_g$  does not effectively constrain the mode width as well as the  $N_T|\sigma_g$  combination. For these reasons, we selected high probability  $N_T|\sigma_g$  combinations to isolate the most probable solutions that could be used to find a unique sea spray mode fit to the measured submicron size distribution

40

## Text S2. Assessment of Sea Spray Retrieval Method using Measured Supermicron Size Distributions

To further assess this new retrieval methodology, we applied the method to a set of clean marine observations from the first cruise of the North Atlantic Aerosols and Marine Ecosystems Study (NAAMES 1) deployed 6 November – 30 November 2015 (Behrenfeld et al., 2019). During NAAMES 1, submicron (0.1 – 0.8  $\mu\text{m}$ ) and supermicron (0.5 – 10  $\mu\text{m}$ ) size distributions  
45 were measured by a Scanning Electrical Mobility Scanner (SEMS, model 2002 BMI) and Aerodynamic Particle Sizer (APS; model 3321 TSI), respectively. Scattering coefficients at  $< 1 \mu\text{m}$  and  $< 10 \mu\text{m}$  diameter cutoffs were measured by a 3- $\lambda$  (450, 550, 700 nm) integrating nephelometer (model 3563, TSI). The availability of the APS provided the ability for our scattering-based approach to be evaluated relative to an external constraint of measured particle size. NAAMES 1 was selected as a case study of the nephelometer constraint on supermicron size because it had the most persistent clean conditions of the four ship  
50 deployments (Saliba et al., 2020). Consequently, the low particle concentrations during NAAMES 1 also saw the lowest sea spray aerosol concentrations of the four NAAMES cruises (Saliba et al., 2019).

(Saliba et al., 2019) merged the NAAMES SEMS and APS measurements (SEMS-APS) to resolve the sea spray size distribution using an automated number concentration fitting algorithm. These size distributions were compared to sea spray  
55 modal properties retrieved with SEMS and nephelometer supermicron scattering (SEMS-NEPH) following the same procedure presented in the main text. Retrieved  $< 10 \mu\text{m}$  SEMS-APS mass during NAAMES 1 was previously compared to size-resolved filter measurements of sodium ( $\text{Na}^+$ ) mass concentration finding a correlation of 0.7, as well as a correlation of 0.6 with wind speed for 15-min averaged data (Saliba et al., 2019). These correlations support the interpretation of the SEMS-APS retrieved mode as sea spray aerosol. Thus, for NAAMES 1, we can provide a direct comparison of sea spray mode retrieval using  
60 supermicron size distributions (SEMS-APS) to the proposed methodology that employs nephelometer scattering to estimate supermicron size (SEMS-NEPH and UHSAS-NEPH).

Figure S6 and Table S1 show comparisons of the SEMS-APS and SEMS-NEPH sea spray retrievals for 2-hr averaged SEMS, APS, and nephelometer measurements. SEMS-NEPH estimates the sea spray mode with double the number concentration, but  
65 only 10% more mass concentration on average than SEMS-APS (Fig. S6a,d). The main differences between these two variables can be explained by the retrieval constraints of each method: SEMS-APS constrains the number size distribution while the Mie-based scattering constraint of SEMS-NEPH is dependent upon the mass concentration. The difference in retrieved number concentrations between the two methods may have implications for attributing particle contributions to CCN. A factor of 2 difference between SEMS-NEPH and SEMS-APS estimates of particle number could modify the observed 10 – 30%  
70 contribution of sea spray to CCN at supersaturations of 0.1 – 0.4% as more particles are contributing to an already low CCN concentration during clean marine conditions (Quinn et al., 2017; Sanchez et al., 2021; Modini et al., 2015).

The majority of integrated mass comparisons fall within a reasonable range of the 1:1 line except for some periods of low SEMS-APS mass concentrations ( $< 3 \mu\text{g m}^{-3}$ ). SEMS-NEPH appears to estimate a larger contribution of scattering from the supermicron aerosol mass that is not observed from the APS during these periods. The larger mass concentration estimates of SEMS-NEPH could be attributable to observed supermicron sea spray mass from the nephelometer that is not fully resolved by the APS number concentration estimate. This is supported by a stronger correlation of retrieved mass with supermicron scattering for SEMS-NEPH ( $R^2 = 0.72$ ) than what is observed using SEM-APS ( $R^2 = 0.56$ ) (Fig S6f), although it should be noted that the supermicron scattering has been used to constrain SEMS-NEPH solutions.

80

Since the width of the sea spray mode from the scattering-based retrieval has been shown to be a poorly constrained parameter and is often narrower for SEMS-NEPH ( $2.0 \pm 0.3$ ) than SEMS-APS ( $2.4 \pm 0.3$ ), it may be the source of discrepancies between the other modal properties (Fig. S6c). These discrepancies are particularly apparent for the mode diameters which are 20% larger in mean number size and 30% smaller in mean mass size for SEMS-NEPH in comparison to SEMS-APS. The scattering-based approach aims to use the probability occurrence of modal width to retrieve an optimal value, but the lack of number size distribution measurements at larger sizes ( $> 0.8 \mu\text{m}$ ) from the SEMS provides insufficient information to constrain this parameter.

For the 2-hr averaged concentrations, sea spray mass concentrations show moderate correlations of 0.50 for SEMS-APS and 0.53 for SEMS-NEPH with wind speed (Fig. S6g). The SEMS-APS correlation of mass to wind speed is slightly weaker than the correlation previously reported by Saliba et al. (2019) for 15-min averages ( $R = 0.6$ ) but remains  $>0.5$  suggesting that the estimated mass concentration from both retrievals can be attributed to sea spray production by wind.

Retrievals of sea salt mass concentration using the supermicron scattering constraint are supported by a moderate correlation ( $R = 0.5$ ) of SEMS-NEPH sea spray mass with ambient  $< 10 \mu\text{m}$  sodium ( $\text{Na}^+$ ) mass analyzed with ion chromatography (Fig. 6h). Although the SEMS-NEPH correlation is weaker than the mass concentration correlation to sodium using SEMS-APS ( $R = 0.7$ ), the SEMS-NEPH result is consistent with other studies merging measured sub- and super-micron size distributions to fit sea spray modes in clean marine conditions (Quinn et al., 2017; Modini et al., 2015).

100

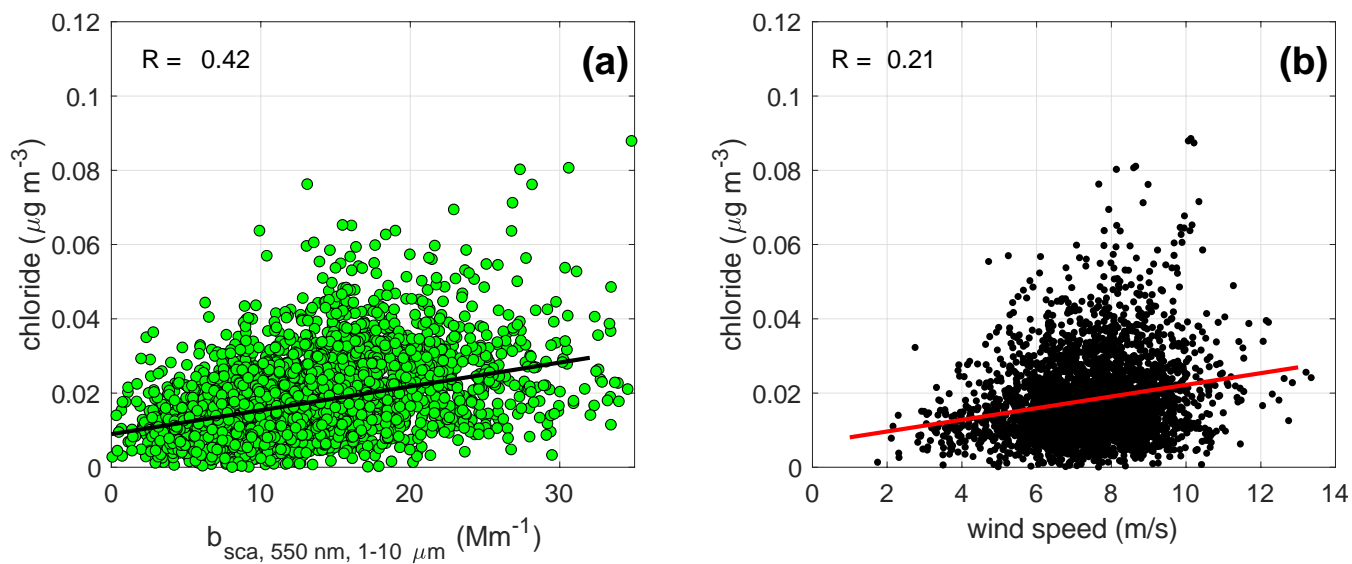


**Figure S1.** (a) Nephelometer supermicron scattering at 550 nm, and (b) wind speed correlations with ACSM chloride concentrations for the period of January 2017 – May 2017 at LASIC. Linear regressions are fit to the data (solid lines) and Pearson correlation coefficients are provided at top left of each panel ( $p < 0.05$ ).

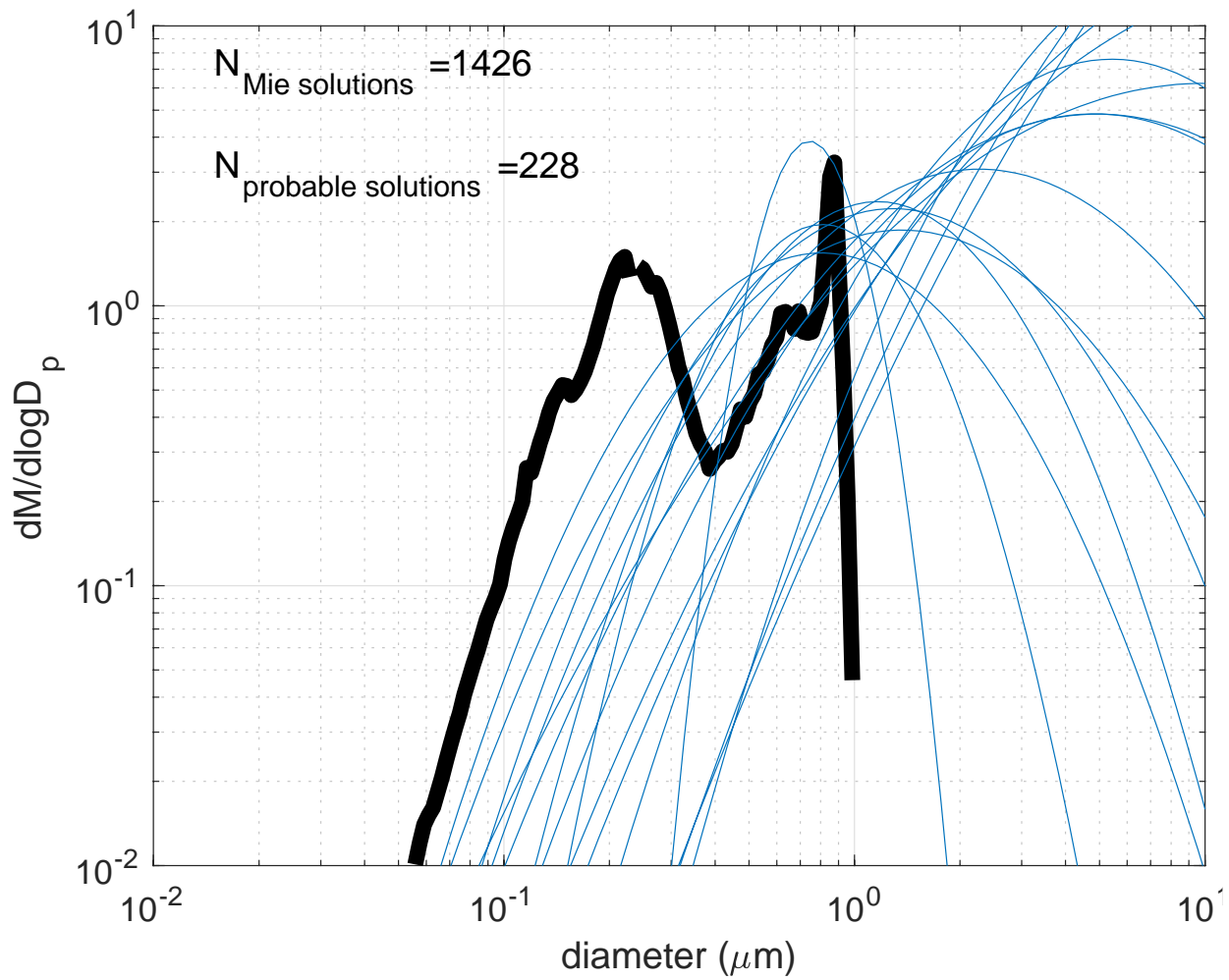
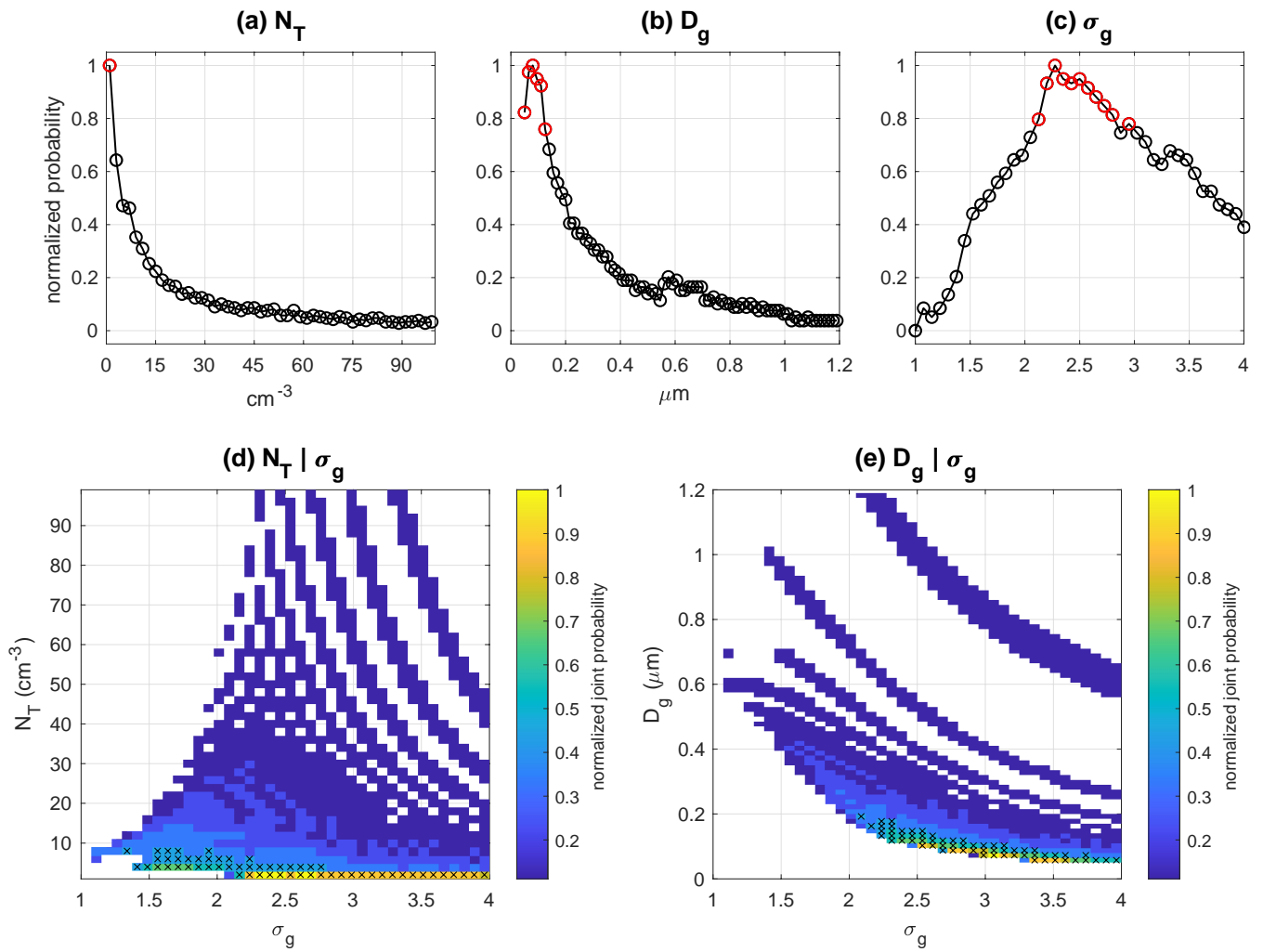


**Figure S2.** Sea spray mode Mie solutions that fall below the retrieval-specific scattering error threshold ( $\Delta\sigma_{sca,RGB}$ ;  $N_{\text{Mie}}$  solutions). The retrieval presented is for the 2-hr average beginning 3 December 2016 22:00 UTC. 1 in every 30 low error Mie solutions are shown to reduce clutter. The size of the reduced solution space for the most probable Mie solutions (Text S2) is identified as  $N_{\text{probable solutions}}$ .



115 **Figure S3.** (a-c) Normalized probability distributions of sea spray mode fitting parameters for low error Mie solutions retrieved during the 2-hr average beginning 3 December 2016 22:00 UTC. Fitting parameter values with an occurrence probability of greater than 75% are symbolized by red circles. (d-e) Normalized joint probability functions (as in color bar) for fitting parameter combinations of  $N_T | \sigma_g$  and  $D_g | \sigma_g$  from the same retrieval. Mie solutions that are within the top 5<sup>th</sup> joint probability percentile for each combination are symbolized by black crosses.

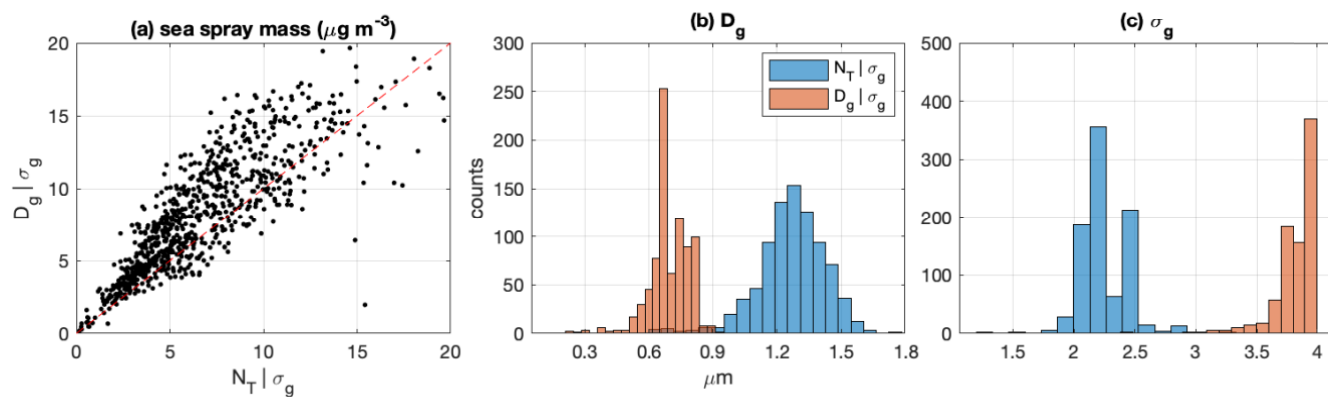


**Figure S4.** Comparisons of retrieved (a) sea spray mass, (b) sea spray mode mass mean diameter ( $\mu\text{m}$ ), and (c) sea spray mode width for joint probability combinations of  $N_T | \sigma_g$  and  $D_g | \sigma_g$  applied to low error Mie solutions (Text S1). In panel (a), the dashed red line symbolizes a 1:1 line.

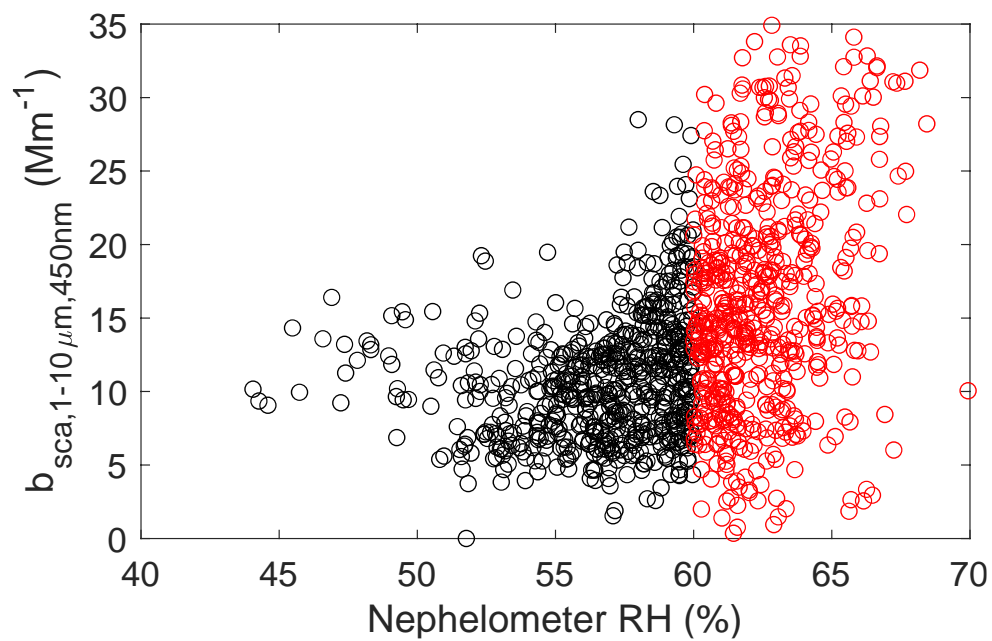
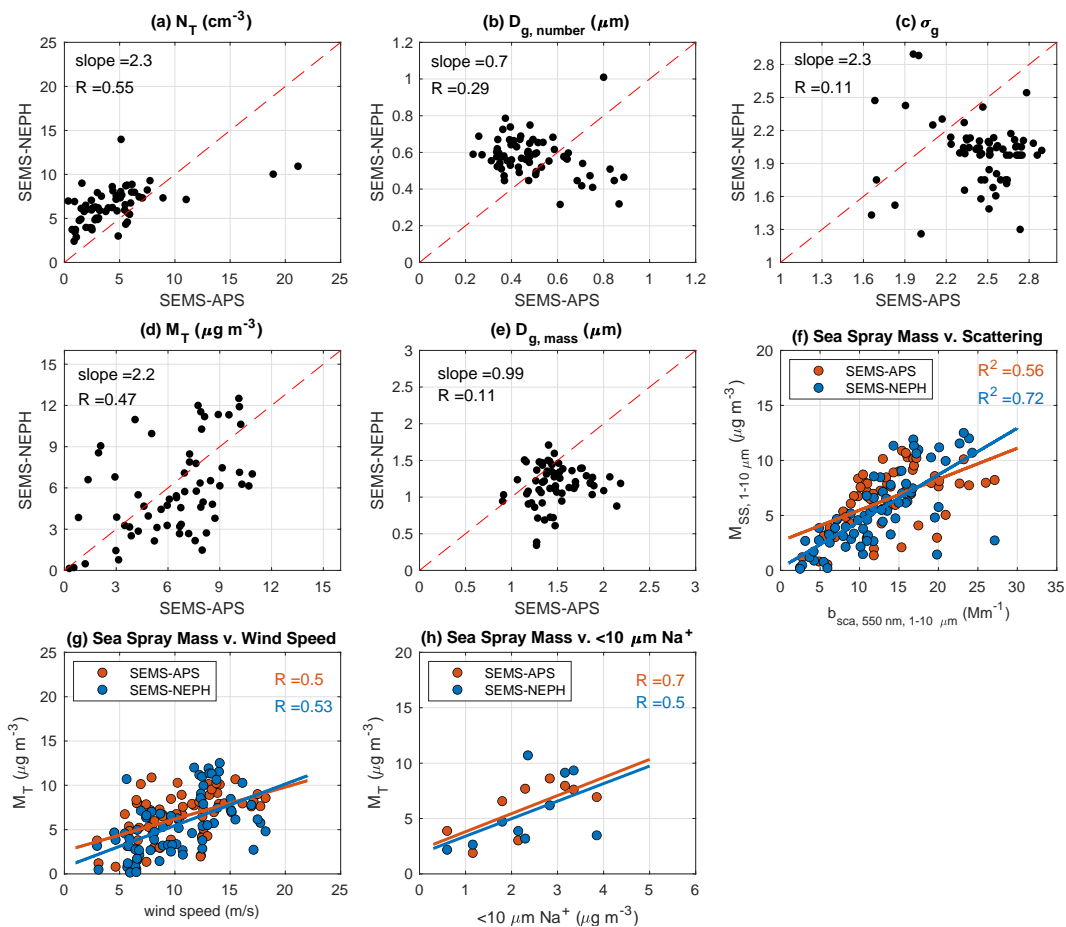


**Figure S5.** Scatter plot of nephelometer control humidity and supermicron scattering at 450 nm ( $\text{Mm}^{-1}$ ). The delineation of black and red data points indicates the restriction used for applicable UHSAS-NEPH sea spray mode retrieval (Section 4).



130

135

140

**Figure S6.** Comparison of retrieved sea spray modal parameters using measured supermicron size distributions (SEMS-APS; Saliba et al., 2019) and Mie inversion of nephelometer supermicron scattering (SEMS-NEPH; this study) during clean marine periods of the NAAMES 1 cruise (6 November – 30 November 2015). 2-hr integrated (a) number ( $\text{cm}^{-3}$ ) and (d) mass ( $\mu\text{g m}^{-3}$ ) concentrations, modal (b) number and (e) mass mean diameters ( $\mu\text{m}$ ), and (c) mode width. (a-e) Slope of linear best fit and Pearson correlation coefficients at top left. Dashed red lines represent a 1:1 line. Sea spray mass correlation with supermicron scattering (f), wind speed (g), and  $<10 \mu\text{m Na}^+$  mass concentration (h) for SEMS-APS (orange) and SEMS-NEPH (blue) methods.  $\text{Na}^+$  mass measurements are from offline filter analysis using ion chromatography. Sea spray mass estimates in (h) are averaged over the filter collection times (24-hr) which provided  $N = 9$  samples. Pearson correlation coefficients (or coefficients of determination) indicated at top right and linear best fit colored by method in (f,g,h).

**Table S1.** Comparison of retrieved sea spray modal parameters using measured supermicron size distributions (SEMS-APS; Saliba et al., 2019) and Mie inversion of nephelometer supermicron scattering (SEMS-NEPH; this study) during clean marine periods of the NAAMES 1 cruise (6 November – 30 November 2015). 2-hr integrated number ( $N_T$ ) concentration, mass concentrations ( $M_T$ ), number mean diameter ( $D_{g,number}$ ), mass mean diameter ( $D_{g,mass}$ ) and mode width ( $\sigma_g$ ). Values are the mean  $\pm$  1 standard deviation.

	$N_T$ ( $\text{cm}^{-3}$ )	$M_T$ ( $\mu\text{g m}^{-3}$ )	$D_{g,number}$ ( $\mu\text{m}$ )	$D_{g,mass}$ ( $\mu\text{m}$ )	$\sigma_g$
<b>SEMS-NEPH</b>	$7.1 \pm 2.1$	$6.1 \pm 2.7$	$0.6 \pm 0.1$	$1.1 \pm 0.3$	$2.0 \pm 0.3$
<b>SEMS-APS</b>	$4.2 \pm 3.4$	$5.5 \pm 3.4$	$0.5 \pm 0.2$	$1.5 \pm 0.3$	$2.4 \pm 0.3$

150

- Behrenfeld, M., Moore, R., Hostetler, C., Graff, J., Gaube, P., Russell, L., Chen, G., Doney, S., Giovannoni, S., Liu, H., Proctor, C., Bolalios, L., Baetge, N., Davie-Martin, C., Westberry, T., Bates, T., Bell, T., Bidle, K., Boss, E., Brooks, S., Cairns, B., Carlson, C., Halsey, K., Harvey, E., Hu, C., Karp-Boss, L., Kleb, M., Menden-Deuer, S., Morison, F., Quinn, P.,  
160 Scarino, A., Anderson, B., Chowdhary, J., Crosbie, E., Ferrare, R., Haire, J., Hu, Y., Janz, S., Redemann, J., Saltzman, E., Shook, M., Siegel, D., Wisthaler, A., Martine, M., and Ziemba, L.: The North Atlantic Aerosol and Marine Ecosystem Study (NAAMES): Science Motive and Mission Overview, *Frontiers in Marine Science*, 6, 10.3389/fmars.2019.00122, 2019.
- Modini, R., Frossard, A., Ahlm, L., Russell, L., Corrigan, C., Roberts, G., Hawkins, L., Schroder, J., Bertram, A., Zhao, R., Lee, A., Abbatt, J., Lin, J., Nenes, A., Wang, Z., Wonaschutz, A., Sorooshian, A., Noone, K., Jonsson, H., Seinfeld, J., Toom-  
165 Sauntry, D., Macdonald, A., and Leaitch, W.: Primary marine aerosol-cloud interactions off the coast of California, *Journal of Geophysical Research-Atmospheres*, 120, 4282-4303, 10.1002/2014JD022963, 2015.
- Quinn, P., Coffman, D., Johnson, J., Upchurch, L., and Bates, T.: Small fraction of marine cloud condensation nuclei made up of sea spray aerosol, *Nature Geoscience*, 10, 674+, 10.1038/NGEO3003, 2017.
- Saliba, G., Chen, C., Lewis, S., Russell, L., Rivellini, L., Lee, A., Quinn, P., Bates, T., Haentjens, N., Boss, E., Karp-Boss, L.,  
170 Baetge, N., Carlson, C., and Behrenfeld, M.: Factors driving the seasonal and hourly variability of sea-spray aerosol number in the North Atlantic, *Proceedings of the National Academy of Sciences of the United States of America*, 116, 20309-20314, 10.1073/pnas.1907574116, 2019.
- Saliba, G., Chen, C., Lewis, S., Russell, L., Quinn, P., Bates, T., Bell, T., Lawler, M., Saltzman, E., Sanchez, K., Moore, R., Shook, M., Rivellini, L., Lee, A., Baetge, N., Carlson, C., and Behrenfeld, M.: Seasonal Differences and Variability of  
175 Concentrations, Chemical Composition, and Cloud Condensation Nuclei of Marine Aerosol Over the North Atlantic, *Journal of Geophysical Research-Atmospheres*, 125, 10.1029/2020JD033145, 2020.
- Sanchez, K., Roberts, G., Saliba, G., Russell, L., Twohy, C., Reeves, M., Humphries, R., Keywood, M., Ward, J., and McRobert, I.: Measurement report: Cloud processes and the transport of biological emissions affect southern ocean particle and cloud condensation nuclei concentrations, *Atmospheric Chemistry and Physics*, 21, 3427-3446, 10.5194/acp-21-3427-  
180 2021, 2021.